Journal of Magnetics 24(1), 24-31 (2019)
ISSN (Print) 1226-1750
ISSN (Online) 2233-6656
https://doi.org/10.4283/JMAG.2019.24.1.024

Influence of Core Stress on Performance of Permanent Magnet Synchronous Motor

Haidong Cao[1], Surong Huang[1]*, and Wenmin Shi[2]

[1]College of Mechatronics Engineering and Automation, Shanghai University, Shanghai 200072, China
[2]National Engineering Research Center for Silicon Steel, Wuhan 430080, China

(Received 6 July 2017, Received in final form 28 December 2018, Accepted 31 December 2018)

The motor core stress produced during the manufacturing process and motor operation changes the electromagnetic characteristics of the iron core. Thus, research on electromagnetic calculations under the condition of stress is one of the key challenges to achieve more efficient designs of permanent magnet motors. In this paper, the stress equations of a rotor centrifuge and stator interference assembly are studied, and the changing regularity of stress and magnetic properties of electrical steel and its causes are analyzed theoretically. A device for measuring the stress and magnetic properties of electrical steel is designed and tested. Then, a model for iron loss calculations that includes stress is proposed for improved design. The effects of stress on loss, *d-q* axis inductance, and torque are simulated and compared using an IPMSM as an example. The feasibility and accuracy of this method are verified by comparing the simulation and prototype test results.

Keywords : permanent magnet motor, core stress, centrifugal force, interference assembly

1. Introduction

Electrical steel is the main magnetic material for motors and crucial for performance and cost. The processing, assembly, and operation of a motor can cause stress on the motor core, which leads to the decline in the magnetic properties of electrical steel, followed by the deterioration of motor performance and increased loss. For modern transportation and industrial applications, the performance index is strict for permanent magnet motors, and material utilization should be maximized in motor design, which poses higher requirements on the application technologies of electrical steel and the accurate calculation of motor iron loss.

In traditional motor design, only the electromagnetic properties of electrical steel under normal conditions are taken into account. As a result, there is significant disagreement between the theoretical results and actual measurements. Research on magnetic properties of electrical steel under the stress field and perform conditions of motor core are lack behind. Moreover, there are insufficient solutions that apply the stress-magnetic properties of electrical steel in the calculation and design of motor properties. This has become one of the main obstacles to designing high-quality permanent magnet motors.

Based on the analysis of the centrifugal stress of a high-speed motor rotor, Jian-xin Shen, He Hao, and Cheng Yuan derived the equation about strain-to-stress relations of rotor under consideration of speed and temperature [1-3]. Miyagi D and other people used the finite element method to simulate the stator core stress generated by the thermal assembly of the motor housing, and derived relations between the thermal assembly temperature and the assembly interference magnitude [4]. In order to analyze the stress-magnetic property of electrical steel, researchers started from the microstructure of electrical steel materials and researched on ferromagnetic property of electrical steel materials, and gave the basic theoretical basis of stress-magnetic property [5]. Laurent Daniel and other scholars conducted experiments on the magnetic properties of electrical steel under stress and concluded that compressive stress in the normal plane can change the magnetic properties of electrical steel; however, they did not study the magnetic properties under tensile stress [6-8]. Yamazaki K and others simulated a surface-mounted permanent-magnet motor on the basis of assembly stress, and verified this simulation method through experiments [9-12]. Daikoku A and other researchers simulated the thermal assembly stress of square housing and housings of different shapes, and analyzed the effect of different

*Corresponding author: Tel: +86-21-5633-5204
Fax: +86-21-5633-3037, e-mail: mtc@shu.edu.cn

housing shapes on cogging torque of the motor [13].

This paper derives the motor stator assembly stress and rotor centrifugal force equation in a cylinder coordinate system. Simulation of the stress field was conducted with the parameters of a prototype motor. The test platform was built to test the magnetic performance under stress conditions from −160 MPa to 160 MPa; in addition, we analyzed the magnetic induction and loss model for electrical steel. The interior permanent-magnet synchronous motor (IPMSM) for vehicles was adopted as the prototype to analyze the performance and parameter changes such as motor torque, loss, efficiency, and *d-q* axis inductance with and without the consideration of motor core stress. The accuracy and feasibility of this method are supported by the comparison between the simulation and observed results.

2. Motor Core Stress Analysis and Calculation

The stress on the stator core is mainly caused by punching, shearing, stacking, nesting, riveting, and welding. The stress, which has the most influential area and the most obvious impact, results from the interference assembly of the motor housing. The main causes of rotor stress on the permanent-magnet motor are the centrifugal force, electromagnetic force, thermal stress, etc. For the IPMSM, owing to the special flux insulation structure of the rotor core, the centrifugal stress is one of the most important influencing factors. The Hooker theorem [14] in the cylindrical coordinate system is expressed as

$$\begin{cases} \varepsilon_r = \dfrac{1}{E}[\sigma_r - \mu(\sigma_\theta + \sigma_z)] \\ \varepsilon_\theta = \dfrac{1}{E}[\sigma_\theta - \mu(\sigma_r + \sigma_z)] \\ \varepsilon_z = \dfrac{1}{E}[\sigma_z - \mu(\sigma_\theta + \sigma_r)] \end{cases} \tag{1}$$

where E is the elastic modulus, μ is the Poisson's ratio, σ_r is the radial stress, σ_θ is the tangential stress, and σ_z is the axial stress.

The motor stator and rotor core axial strain are negligible in the actual calculation, compared with the radial and tangential strain. Thus, the radial, tangential, and axial stress equations of the motor are as follows:

$$\begin{cases} \sigma_r = \dfrac{E(1-\mu)}{(1+\mu)(1-2\mu)}\dfrac{\mathrm{d}s}{\mathrm{d}r} + \dfrac{E\mu}{(1+\mu)(1-2\mu)}\dfrac{s}{r} \\ \sigma_\theta = \dfrac{E\mu}{(1+\mu)(1-2\mu)}\dfrac{\mathrm{d}s}{\mathrm{d}r} + \dfrac{E(1-\mu)}{(1+\mu)(1-2\mu)}\dfrac{s}{r} \\ \sigma_z = \mu(\sigma_r + \sigma_\theta) \end{cases} \tag{2}$$

where s is the radial displacement.

The Fontaineus stress (equivalent stress) is obtained as follows:

$$\sigma = \sqrt{\frac{1}{2}[(\sigma_r - \sigma_\theta)^2 + (\sigma_\theta - \sigma_z)^2 + (\sigma_z - \sigma_r)^2]} \tag{3}$$

The interference assembly of the stator core and motor housing cause the stator core stress. The assembly interference magnitude can be formulated as follows:

$$\delta_s = R_s - r_f \tag{4}$$

where R_s is the outer radius of the stator core, and r_f is the inner radius of the motor housing.

The analytical equation [15] of the stator core produced by the assembly interference is

$$P_s = \frac{\delta_s}{R_s\left[\dfrac{1}{E_h}\left(\dfrac{R_s^2 + R_h^2}{R_s^2 - R_h^2} + \mu_h\right) + \dfrac{1}{E_s}\left(\dfrac{r_s^2 + R_s^2}{R_s^2 - r_s^2} - \mu_s\right)\right]} \tag{5}$$

where r_s is the stator yoke radius, R_f is the outer radius of the chassis, P_s is the stator core in the radial direction of the housing pressure; E_s, E_h are the Young's modulus of the core and shell, and μ_s, μ_h are the core and housing Poisson's ratio, respectively.

The balance equation [16] for the centrifugal stress of the rotor is

$$\frac{\mathrm{d}\sigma_r}{\mathrm{d}r} + \frac{\sigma_r - \sigma_\theta}{r} + \rho\omega^2 r = 0 \tag{6}$$

where ω is the motor speed, and ρ is the core density.

3. Experiment and Research on Stress and Magnetic Property of Electical Steel

The test determined the stress-magnetic properties of electrical steel. The rule of changes was analyzed, which

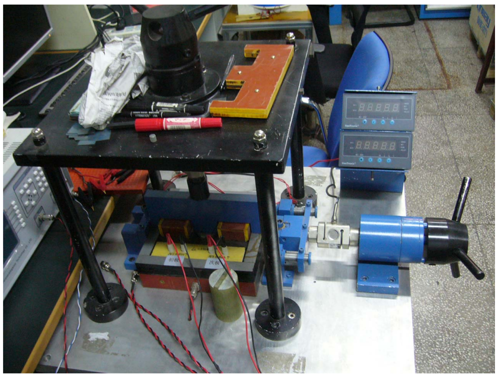

Fig. 1. (Color online) E-steel test platform for stress-magnetic property.

is the basis of the electromagnetic calculation model of electrical steel, including the stress condition. A double yoke structure test platform for the stress and magnetic properties of electrical steel was designed by the author's research team in order to apply the compressive (tensile) stress and normal compressive stress in the normal plane direction, as shown in Fig. 1.

In this experiment, in order to test and analyze the loss and magnetic induction characteristics of electrical steel in the stress range from −160 MPa to 160 MPa (in elasticity, the compression is negative while the tension is positive). A 0.35 mm thick non-oriented electrical steel was selected as the research object.

3.1. Cause and Changing Regularity of Stress and Magnetic Property

The cause that the iron core magnetic property varies with stress can be analyzed from two aspects: magnetoelastic property and stress demagnetization. According to the ferromagnetism theory, when exert the uniaxial stress σ over ferromagnetic crystal materials, the magnetoelastic energy can be expressed by the formula:

$$E_o = \frac{3}{2}\lambda_s \sigma^2 \sin^2\theta \tag{7}$$

where λ_s is the magnetostrictive coefficient, σ is the uniaxial stress, and θ is the angle between the stress and magnetization.

For electrical steel, $\lambda_s > 0$, the magnetoelastic energy E_σ is minimum, and the direction of magnetization changed to the direction of tension, which facilitates magnetization under the tensile stress condition (when $\sigma > 0$), if $\theta = 0°$. The magnetoelastic energy E_σ is also minimum under the compressive stress condition (when $\sigma < 0$), if $\theta = 90°$. However, magnetization is hindered, thus the magnetic conductivity of electrical steel declines.

Whereas in fact, stress changes the grain orientation and position, from the point of stress demagnetization, at the meanwhile, produces a magnetic field with opposite demagnetizing field along the crystal surface.

Under the condition of tensile stress, little change occurs in the demagnetizing field; with increasing stress, the demagnetizing field straights up.

For soft magnetic materials, the coercivity H_c and remanence B_r are two important evaluation indexes that determine the reversal magnetization process and loss properties of materials.

The Jiles–Atherton domain wall displacement model [17] is shown as formula (8), considering the stress field

$$H_e = H + \alpha M + \frac{M}{M_s}\frac{3\lambda_s\sigma}{\mu_0 M_s}\cos^2(\theta_\sigma - \theta_H) \tag{8}$$

where λ_s is saturation magnetostrictive coefficient, M is the system magnetization, and M_s is the system saturation magnetization.

The coercivity H_{cr} is mainly related to magnetic anisotropy in the domain wall rotation magnetization mechanism. The Stoner–Woflrath domain rotation model is shown as formula (9), considering the interaction between the stress and external magnetic field.

$$H_{eff} = H + \alpha\langle M\rangle \tag{9}$$

where α is the mean field interaction coefficient, and $\langle M\rangle$ is average magnetization of the system.

3.2. Stress and Magnetic Property Test

The magnetic induction properties of electrical steel in the stress range from −80 MPa to 80 MPa were tested, as shown in Fig. 2.

The experimental results show that under the condition of compressive stress, the demagnetization factor is always dominant, and the magnetic permeability of electrical steel decreases monotonously. Under the condition of tensile stress from 0 MPa to 20 MPa, the factors of the magnetoelastic property dominate, while magnetic induction increases slightly. When the tensile stress exceeds 20 MPa, the factors of stress demagnetization gradually dominate while magnetic conductivity decreases.

Under the conditions of different stress, the loss characteristics of electrical steel are shown in Fig. 3.

The experimental results show that under the condition of compressive stress, the displacement mechanism of the domain wall plays a dominant role, and the value of electrical steel loss rises monotonically. Under the condition of tensile stress from 0 MPa to 20 MPa, the magnetization reversal mechanism is mainly the domain wall displacement mechanism, and the coercivity and iron loss decrease.

When the tensile stress exceeds 20 MPa, the magnetization reversal mechanism is mainly the domain rotation

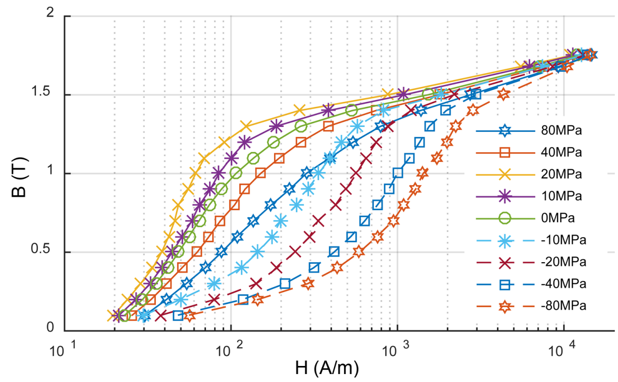

Fig. 2. (Color online) Effect of stress on magnetic induction.

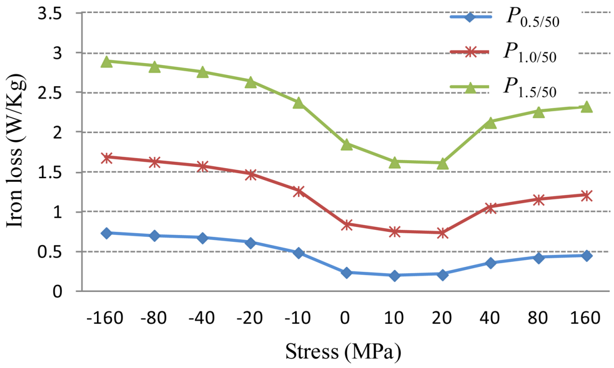

Fig. 3. (Color online) Effect of stress on iron loss.

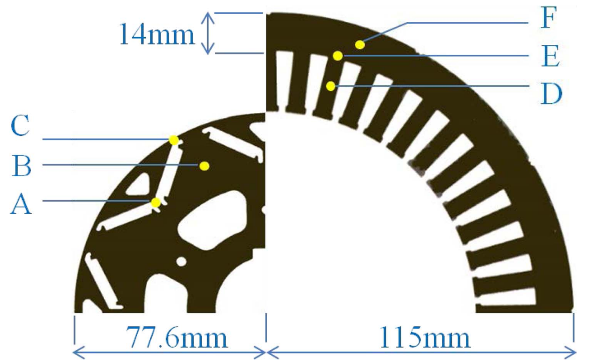

Fig. 4. (Color online) Iron core structure (main parameters and representative part A-E of the iron core).

mechanism, and the anisotropy of electrical steel increases as well as the coercivity and iron loss.

The magnetic induction characteristic of electrical steel in the stress field can be expressed as

$$B = \mu_\sigma H \tag{10}$$

where μ_σ is magnetic conductivity in the stress field, which can be obtained by the magnetic induction test curve of the material under the stress condition.

Motor iron loss is usually calculated using the Bertotti iron dissipation model

$$P_{\mathrm{Fe}} = k_h f B^\alpha + k_e f^2 B^2 + k_{ex}(fB)^{\frac{3}{2}} \tag{11}$$

where k_h is the hysteresis loss coefficient, k_e is the eddy loss coefficient, k_{ex} is the additional loss coefficient, α is the undetermined coefficient from 1.6 to 2.2, and coefficients k_h, k_e, k_{ex}, α depend on the characteristics of electrical steel.

Based on the impact of stress on electrical steel loss properties, the model of the separation of iron loss in the stress field was obtained by introducing the stress and iron loss correction coefficients $\beta_{1\sigma}$ and $\beta_{2\sigma}$, respectively, which are associated with principal stress.

$$P_{\mathrm{Fe}} = k_h \beta_{1\sigma} f B^\alpha + k_e f^2 B^2 + \beta_{2\sigma} k_{ex}(fB)^{\frac{3}{2}} \tag{12}$$

In the formula, $\beta_{1\sigma}$ and $\beta_{2\sigma}$ are the correction coefficients of hysteresis loss and additional loss under stress impact, respectively. $\beta_{1\sigma}$ and $\beta_{2\sigma}$ can be obtained from the loss test curve under the stress condition. k_h, k_e, k_{ex}, α are the coefficients of the original Bertotti iron loss separation model.

4. Influence of Core Stress on Motor Performance

The advantages and disadvantages of iron core magnetic properties directly affect the motor magnetic field distribution, torque, inductance, etc. The iron loss characteristics of the iron core also directly affect the loss and efficiency of the motor. On the basis of the study on the stress of electrical steel and the calculation of the stress on the stator and rotor core, the electromagnetic field and performance were simulated.

We used a three-phase, vehicle used traction IPMSM as a prototype for the simulation and analysis in this study. Fig. 4 shows the iron core structure and main size parameters for improved analysis, and the representative parts A–E of the iron core are selected.

4.1. Stress Simulation of IPMSM Core

The motor assembly interference magnitude δ_s is 0.08 mm. According to formulas (1)–(6), we simulated the assembly stress on the stator core and rotor centrifugal stress at 10000 r/min. The results are shown in Fig. 5.

It is clear that the stress caused by the rotor centrifugal force is tensile stress, which is present in the entire rotor core. The maximum centrifugal stress occurs in the motor rotor isolation bridge and stiffener ribs with values ranging from 50 MPa to 110 MPa, as shown in Fig. 5. The stator core stress, which is caused by the interference assembly of the motor housing, is compressive stress that

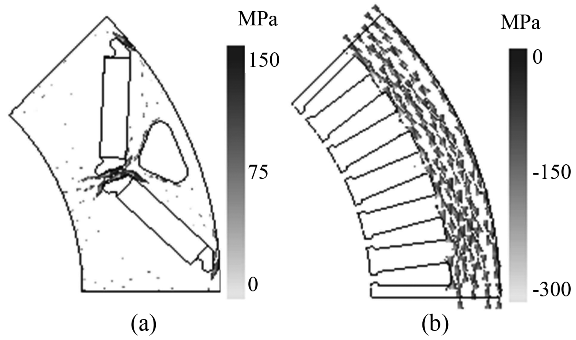

Fig. 5. (Color online) Calculated principal stress distribution: (a) Rotor core, (b) Stator core.

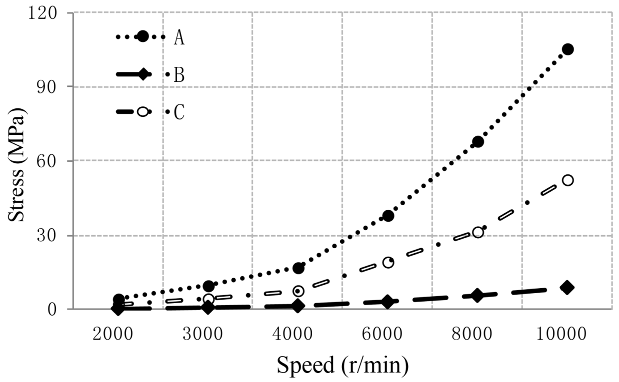

Fig. 6. Rotor centrifugal stress under different rotational speed.

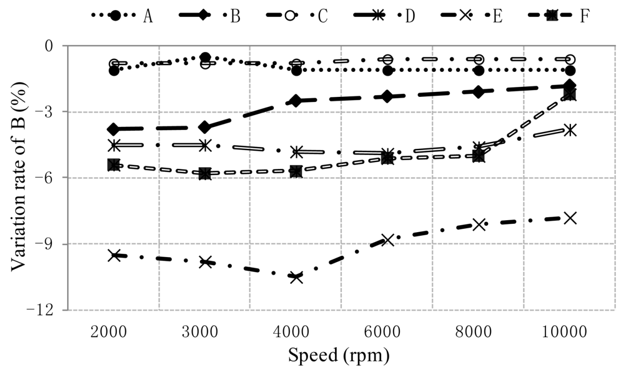

Fig. 8. Magnetic density variation rate caused by stress.

exists mainly in the stator yoke; along the circumference, the principal stress direction is the tangential direction.

Figure 6 shows that with increasing speed, the centrifugal stress of the rotor core increases steadily, which is consistent with the result of formula (6). Point B, which represents the state of stress in most of the area, is always below 10 MP. Owing to the effect of centrifugal stress, the motor rotor loss of electromagnetic performance is improved.

4.2. Influence of Core Stress on Motor Magnetic Field

The relative permeabilities of the iron core and magnetic field of the IPMSM were calculated based on the results of the stator and rotor core stress simulation. The relative permeability distribution of the stator and rotor core is shown in Fig. 7.

As a result of the existence of the stress field, the relative permeability distribution of the stator and rotor iron core changed. Compared with the rotor core, the change in the relative magnetic permeability of the stator is more apparent. The variation of the magnetic density of the typical A-E position is analyzed in Fig. 8.

Figure 8 shows that the change in the magnetic density of the stator iron core is significant. On the other hand, the change in the magnetic density of the motor magnetic bridge and strengthening ribs is smallest because the magnetic field has been saturated. The simulation also shows that the change in magnetic density is dramatically greater than that at high speed when the motor speed is below 4000 r/min.

4.3. Influence of Core Stress on Iron Loss

The simulation result for iron loss distribution of the motor at 4000 r/min is shown in Fig. 9. From the diagram, the iron loss of the stator core obviously increases when considering the stress, especially in the stator yoke.

In order to better analyze the change in iron loss caused

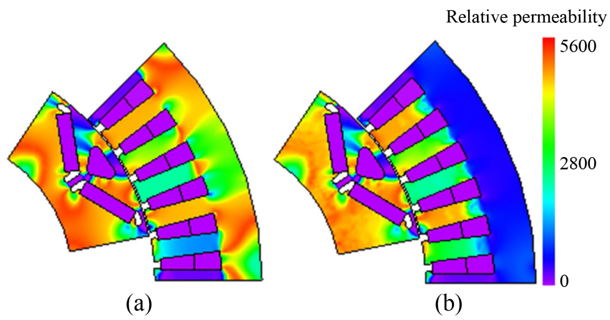

Fig. 7. (Color online) Calculated relative permeability distribution: (a) Without stress, (b) With stress.

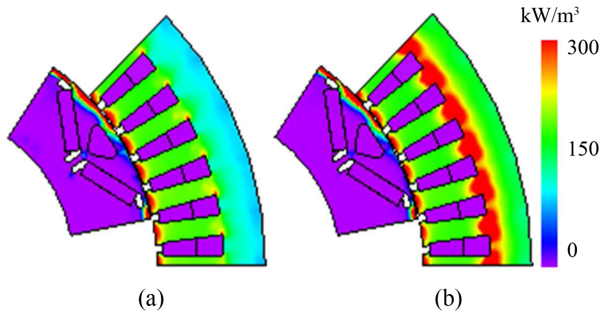

Fig. 9. (Color online) Distribution of the iron loss: (a) Without stress, (b) With stress.

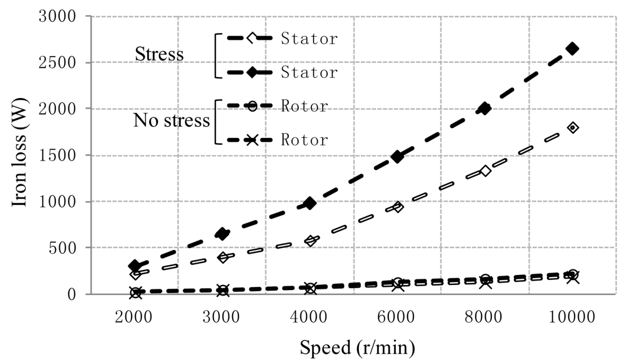

Fig. 10. Influence of stress on core loss.

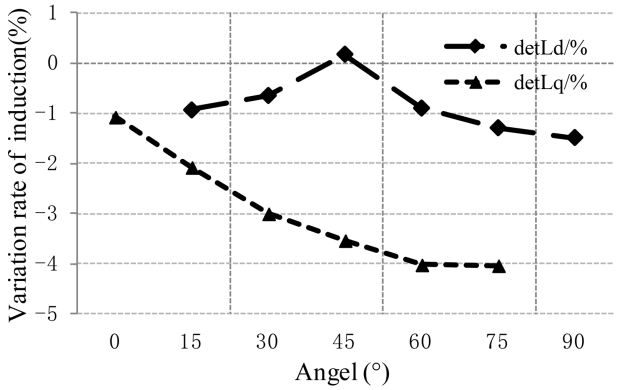

Fig. 11. Induction variation rate caused by stress.

by iron core stress, the losses in various parts of the motor from 2000 r/min to 10000 r/min were calculated, as shown in Fig. 10.

The simulation results show that the stator iron loss increased significantly from 2000 r/min to 10000 r/min under the iron loss condition of the stator core loss calculation model. Compared with the traditional model of iron loss, the rotor iron loss decreased slightly. Because the stator iron loss is greater than the rotor iron loss, the total iron consumption of the motor increased significantly considering stress.

Stress changed the iron core permeability and loss performance of the motor. Thus, it affects the magnetic resistance and inductance parameters of the motor magnetic circuit, main magnetic flux, and leakage flux values. Based on the calculated results of the stress field, the electrical inductance of the motor *d-q* axis with the current angle was simulated. The results are shown in Fig. 11.

The inductance of the *d-q* axis decreased, especially the inductance of the *q*-axis, because of the deterioration of the magnetic inductance property in response to stress. According to the analysis of the magnetic circuit, the *d*-axis magnetic circuit contains the air gap, permanent magnets, and stator iron core. Among them, the permanent magnets are the main factor. Hence, the change in *d*-axis inductance caused by the magnetic inductance property is not obvious. The *q*-axis magnetic circuit consists of the stator iron core and air gap, which means that the magnetic resistance is much smaller compared with permanent magnets. Therefore, the magnetic induction property will deteriorate while *q*-axis induction presents a decreasing trend, considering the core stress. The electromagnetic torque of the permanent magnet motor can be expressed as

$$T_{em} = p[\psi_f i_q + (L_d - L_q) i_d i_q] \tag{13}$$

where L_d and L_q are *d-q* axis inductance, i_d and i_q are the *d-q* axis current, p is the motor pole pairs, and ψ_f is the flux linkage produced by the permanent magnet.

The electromagnetic torque of the motor is related to the *d-q* axis inductance and flux linkage ψ_f. When calculating the impact of stress-magnetic properties, the magnetic inductance of the motor iron core and flux linkage ψ_f will decrease; at the same time, the difference between L_d and L_q decreases. All of the above conditions will lead to the reduction of the electromagnetic torque of the permanent-magnet motor. The simulation results show that the electromagnetic torque of the IPMSM decreased when calculating the stress-magnetic effect, the details of which are shown in Fig. 13.

5. Experimental Verification of Prototype Machine

To verify the feasibility of this method, the torque and efficiency index of an IPMSM drive for a vehicle were tested in this study. The prototype machine test platform is shown in Fig. 12.

When the machines are operating within the speed range of 2000 r/min to 10000 r/min, the motor torque T various rate of simulation compared with experimental

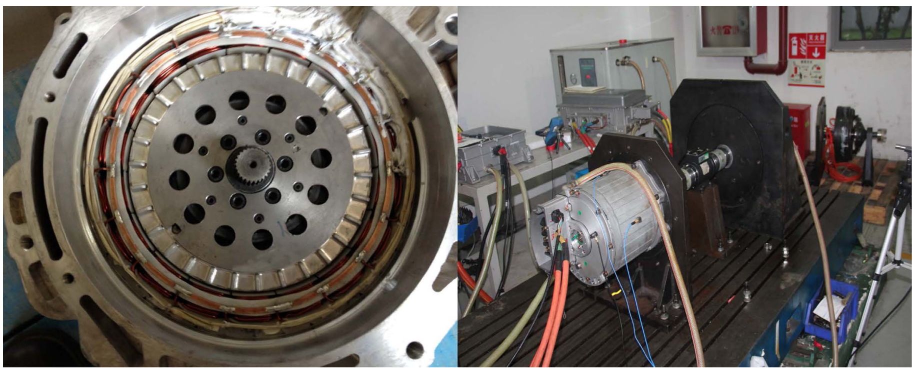

Fig. 12. (Color online) Prototype machine and test platform.

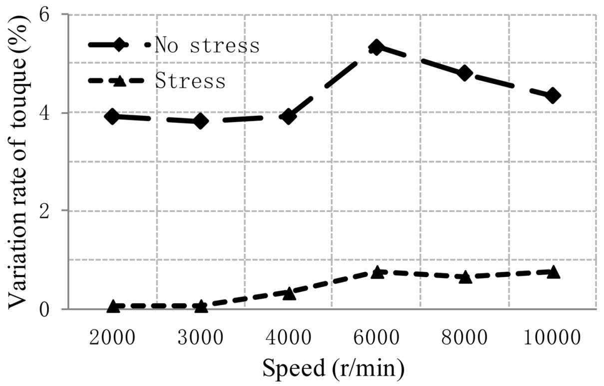

Fig. 13. Variation rate between simulated torque and tested torque.

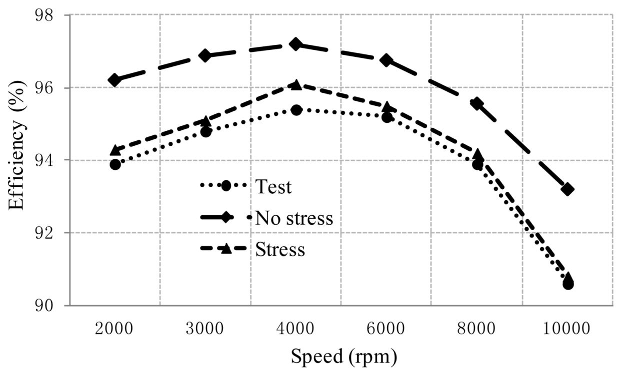

Fig. 14. Efficiency of IPMSM under different rotational speed.

value is shown in Fig. 13.

It shows that the simulation result is very close to the actual value of the impact force for the whole range of motor speeds, considering the motor torque force influence of iron core stress. The maximum error is less than 0.8%.

The simulated efficiency of the IPMSM at different speeds is shown in Fig. 14. In the simulation, the mechanical loss of the motor was calculated by formula (14).

$$P_{smooth} = kC_f \pi \rho \omega^3 r^4 l \tag{14}$$

where k is the rotor surface roughness; p is the air density; ω, r, l are the rotor angular speed, rotor radius, and axial length, respectively; and C_f is the air friction coefficient, which is related to the rotor surface shear force.

As shown in Fig. 14, by considering the effect of stress, the calculated results for motor efficiency η are closer to the experimental values. The data proved the feasibility and accuracy of the calculation and simulation methods described in this study.

6. Conclusion

In this study, we first derived the relation between the assembly stress on a stator and the centrifugal stress on a rotor in a cylindrical coordinate system. We also simulated the stress field according to experimental prototype parameters. Secondly, we tested the magnetic properties of electrical steel under stress ranging from −160 MPa to 160 MPa using a test platform of the stress-to-magnetic properties of electrical steel. We also simulated the loss and magnetic properties of electrical steel subjected to stress. Thirdly, we simulated the changes in the performance and parameters of motor torque, loss, efficiency, and *d-q* axis inductance with or without considering the stator stress by studying an IPMSM. Finally, we proved the accuracy and feasibility of this method by comparing the simulation results with experimental data for a prototype operation. The results are as follows:

1) Both theoretical and experimental analyses showed that the performance of electrical steel declined when the pulling stress and crushing stress is greater than 20 MPa. However, the performance of electrical steel can be improved when the pulling stress ranges from 0 MPa to 20 MPa.

2) The stator and rotor core stress analysis equations in the cylindrical coordinate system were used to simulate and calculate the stress distribution in the stator and rotor core. The results show that the flux insulation bridge and rib of the IPMSM rotor and yoke of the stator are the main areas where stress accumulates, and the values are associated with motor speed as well as the assembly interference magnitude.

3) The electromagnetic performance of the permanent magnet motor was simulated based on the calculated results of the stress field. It was found that the core stress affected the magnetic field, iron loss distribution, flux isolation bridge, leakage flux, and L_d and L_q.

4) The calculation values of IPMSM torque and loss are more accurate and closer to actual working conditions when the effect of core stress is included, after comparing the experimental results with the simulation results. The method including the effect of core stress can be used to improve the design and calculation of permanent magnet motors.

Acknowledgments

This work was supported by Key Project of the National Research Programme of China (2018YFB0104704, 2015BAG03B01), and Ford global university cooperation project (URP, 2013-7060R).

References

[1] J. Shen, H. Hao, and C. Yuan, P. CSEE **32**, 53 (2012).

[2] Daisuke Miyagi, Kohei Miki, Masanori Nakano, and Norio Takahashi, IEEE Trans. Magn. **46**, 318 (2010).
[3] Jae-Woo Jung, Byeong-Hwa Lee, Do-Jin Kim, Jung-Pyo Hong, Jae-Young Kim, Seong-Min Jeon, and Do-Hoon Song, IEEE Trans. Magn. **48**, 911 (2012).
[4] Daisuke Miyagi, Noriko Maeda, Yuki Ozeki, Kouhei Miki, and Norio Takahashi, IEEE Trans. Magn. **45**, 1704 (2009).
[5] André Thiaville, J. Magn. Magn. Mater. **182**, 5 (1998).
[6] Laurent Daniel1 and Olivier Hubert, J. Appl. Phys. **105**, 2113 (2009).
[7] K. Fujisaki and S. Satoh, IEEE Trans. Magn. **40**, 1820 (2004).
[8] M. Kawabe, T. Nomiyama, A. Shiozaki, M. Mimura, N. Takahashi, and M. Nakano, IEEE Trans. Magn. **48**, 3462 (2012).
[9] Katsumi Yamazaki and Yusuke Kato, IEEE Trans. Magn. **50**, 909 (2014).
[10] Katsumi Yamazaki and Yuya Sakurai, "18th International Conference on Electrical Machines and Systems (ICEMS)" (2015).
[11] Laurent Bernard and Laurent Daniel, IEEE Trans. Magn. **51**, 1 (2015).
[12] A. Daikoku, M. Nakano, S. Yamaguchi, Y. Tani, Y. Toide, H. Arita, T. Yoshioka, and C. Fujino, "IEEE International Conference on Electric Machines and Drives (IEMDC)" (2005).
[13] D. L. Atherton and J. R. Beattie, IEEE Trans. Magn. **26**, 3059 (1990).
[14] C. Zhang, J. Zhu, and X. Han, P. CSEE, **36**, 4719 (2016).
[15] F. Zhang, G. Du, T. Wang, and N. Huang, P. CSEE **33**, 195 (2013).
[16] C. Feng, L. Yi, P. Liang, and Y. Pei, IEEE Trans. Ind. Electron. **63**, 3420 (2016).
[17] Keisuke Fujisaki, Ryu Hirayama, Takeshi Kawachi, Shouji Satou, Chikara Kaidou, Masao Yabumoto, and Takeshi Kubota, IEEE Trans. Magn. **43**, 1950 (2007).